Theor Appl Genet (2013) 126:159–177
DOI 10.1007/s00122-012-1970-z

ORIGINAL PAPER

Paramutagenicity of a *p1* epiallele in maize

Wolfgang Goettel · Joachim Messing

Received: 28 June 2012 / Accepted: 16 August 2012 / Published online: 18 September 2012

Abstract Complex silencing mechanisms in plants and other kingdoms target transposons, repeat sequences, invasive viral nucleic acids and transgenes, but also endogenous genes and genes involved in paramutation. Paramutation occurs in a heterozygote when a transcriptionally active allele heritably adopts the epigenetic state of a transcriptionally and/or post-transcriptionally repressed allele. *P1-rr* and its silenced epiallele *P1-pr*, which encode a *Myb*-like transcription factor mediating pigmentation in floral organs of *Zea mays*, differ in their cytosine methylation pattern and chromatin structure at a complex enhancer site. Here, we tested whether *P1-pr* is able to heritably silence its transcriptionally active *P1-rr* allele in a heterozygote and whether DNA methylation is associated with the establishment and maintenance of *P1-rr* silencing. We found that *P1-pr* participates in paramutation as the repressing allele and *P1-rr* as the sensitive allele. Silencing of *P1-rr* is highly variable compared to the inducing *P1-pr* resulting in a wide range of gene expression. Whereas cytosine methylation at *P1-rr* is negatively correlated with transcription and pigment levels after segregation of *P1-pr*, methylation lags behind the establishment of the repressed *p1* gene expression. We propose a model in which *P1-pr* paramutation is triggered by changing epigenetic states of transposons immediately adjacent to a *P1-rr* enhancer sequence. Considering the vast amount of transposable elements in the maize genome close to regulatory elements of genes, numerous loci could undergo paramutation-induced allele silencing, which could also have a significant impact on breeding agronomically important traits.

Communicated by B. Friebe.

Electronic supplementary material The online version of this article (doi:10.1007/s00122-012-1970-z) contains supplementary material, which is available to authorized users.

W. Goettel · J. Messing (✉)
Waksman Institute of Microbiology, Rutgers University,
190 Frelinghuysen Road, Piscataway, NJ 08854, USA
e-mail: messing@waksman.rutgers.edu

Introduction

Paramutation is an epigenetic silencing phenomenon that occurs between homologous or allelic sequences (Arteaga-Vazquez and Chandler 2010; Chandler 2010; Chandler and Stam 2004; Erhard and Hollick 2011; Hollick 2010). Several epialleles—alleles that share an identical nucleotide sequence but differ in their epigenetic state—have been shown to participate in paramutation. Paramutation or paramutation-like silencing events have also been reported between two transgenes, and between transgenes and endogenous genes. Paramutation is defined as the interaction of two alleles in a heterozygote where one allele is able to reduce heritably the expression status of another allele. Consequently, paramutation is a violation of Mendel's First Law, stating that genes leave a heterozygote without having influenced each other. The inducing allele in the heterozygote possessing the repressive function is called paramutagenic, whereas the sensitive allele that is heritably silenced is termed paramutable. The paramutable allele, after exposure to the paramutagenic allele, is referred to as paramutant allele and is usually marked with a prime (′). Neutral alleles are neither paramutagenic nor paramutable, they simply do not participate in paramutation. Paramutation represents an important system to study establishment, maintenance, and inheritance of epigenetically regulated genes.

Brink discovered paramutation in maize more than 50 years ago and published his first report on paramutation at the *r1* (*red1*) locus (Brink 1956). Brink coined the term paramutation (para, Greek: beside, near, beyond, aside) in 1958 (Brink 1958) to contrast paramutation with mutation. Paramutation occurs under specific conditions and is always directed, while mutations resulting in reduced gene expression are sporadic and indirect. While paramutation is best characterized in maize it has been described in several plant, fungi and animals species (Brink 1973; Chandler and Stam 2004). For instance, paramutation or paramutation-like effects were found in tomato (*Lycopersicon esculentum*) (Ehlert et al. 2008), *Arabidopsis thaliana* (Mittelsten Scheid et al. 2003; Stokes and Richards 2002), petunia (*Petunia hybrida*) (Meyer et al. 1993), snapdragon (*Antirrhinum majus*) (Krebbers et al. 1987), garden pea (*Pisum sativum*) (Bateson and Pellew 1915), *Ascobolus immersus* (Colot et al. 1996) and more recently in mice (*Mus musculus*) (Cuzin et al. 2008; Grandjean et al. 2009; Rassoulzadegan et al. 2006, 2007; Wagner et al. 2008; Worch et al. 2008).

To date, five loci in maize, namely *r1* (*red1*) (Brink 1956; Kermicle et al. 1995; Walker 1998), *b1* (*booster1*) (Coe 1966; Stam et al. 2002), *pl1* (*purple plant1*) (Hollick et al. 1995), *p1* (*pericarp color1*) (Sidorenko and Chandler 2008; Sidorenko and Peterson 2001) and *lpa1* (*low phytic acid1*) (Pilu et al. 2009), have been shown to participate in paramutation. Four of them encode transcriptional regulators that activate structural genes in the anthocyanin biosynthesis pathway. Accordingly, they control the accumulation of purple anthocyanin and red phlobaphene pigments in vegetative, floral and seed tissue, which results in a readily visible phenotype. R1 and B1 are members of the Myc-class of basic helix-loop-helix DNA binding proteins, whereas PL1, C1 and P1 are Myb-like transcription factors. The fifth gene, *lpa1*, encodes a transmembrane transporter involved in phytic acid metabolism. Whereas paramutation at *r1*, *b1*, *pl1* and *p1* leads to a reduction in easily visible but dispensable pigments, silencing of the essential *lpa1* gene in contrast is lethal.

A major breakthrough in the understanding of paramutation and epigenetic gene regulation in maize has been the isolation of mutants that disrupt the silencing pathways of numerous epigenetic phenomena. Several *mediator of paramutation* (*mop*) and *required to maintain repression* (*rmr*) mutants have been isolated employing the B' and Pl' alleles, respectively. *mop1* encodes an RNA-dependent RNA polymerase (RDR), which is similar to *RDR2* in Arabidopsis (Alleman et al. 2006). *mop2*, also known as *rmr7* is homologous to the Arabidopsis *NRPD2/E2* and codes for one of the second-largest subunits of the plant-specific RNA polymerases IV and V (Sidorenko et al. 2009; Stonaker et al. 2009). The largest subunit of the putative maize Pol IV is encoded by *rmr6* and is closest to Arabidopsis *NRPD1* (Erhard et al. 2009). *rmr1* encodes a presumed chromatin-remodeling protein that contains a Sucrose Nonfermenting2 (SNF2) and a helicase domain (Hale et al. 2007). *rmr1* shares sequence similarities with Arabidopsis *CLASSY1* (*CLSY1*) and *DEFECTIVE IN RNA-DIRECTED METHYLATION1* (*DRD1*). Interestingly, homologs of the *rmr* and *mop* genes in Arabidopsis are involved in the RNA-directed DNA methylation (RdDM) pathway that leads to DNA methylation, chromatin modifications, and transcriptional gene silencing. Small interfering RNAs (siRNAs) that are generated in the course of RdDM could at least partially account for allelic interactions between the paramutagenic and paramutable alleles (Arteaga-Vazquez et al. 2010; Arteaga-Vazquez and Chandler 2010).

The paramutable *R-r:std* (*R-r:standard*) and *R-d* (*R-d:Catspaw*) alleles and the paramutagenic *R-st* (*R-stippled*) and *R-mb* (*R-marbled*) alleles that participate in *r1* paramutation are structurally very distinct (Chandler et al. 2000). In contrast, the paramutable *B-I* (*booster-Intense*) and the paramutagenic B' alleles that are involved in *b1* paramutation are epialleles. Their nucleotide sequences are identical over a region of 150 kb, including the seven direct tandem repeats of 853 bp that are necessary for enhancer function and paramutation (Stam et al. 2002). *r1* and *b1* alleles that participate in paramutation have one common denominator: they contain sequences that are duplicated. Intriguingly, paramutagenicity is correlated with the number of various repetitive sequences in *R-st* (Kermicle et al. 1995), *R-mb* (Panavas et al. 1999), and B' (Stam et al. 2002). Most if not all species investigated, including prokaryotes, seem to possess a mechanism that targets duplicated sequences for silencing. In eukaryotes, repeat-induced silencing leads to the formation of repressive chromatin structure and DNA methylation, which correlate with suppression of transcription and recombination (Dooner and He 2008; Law and Jacobsen 2010; Maloisel and Rossignol 1998). Indeed, B' has a different chromatin structure and methylation pattern than *B-I* at repeats (Haring et al. 2010), and the paramutant *R-r:std* allele is methylated at the doppia transposon required for *R-r:std* transcription in the aleurone layer (Walker 1998).

Several naturally occurring alleles of the *p1* gene with repeat arrangements are also epigenetically controlled (Das and Messing 1994; Goettel and Messing 2009; Robbins et al. 2009; Sekhon and Chopra 2009; Sekhon et al. 2007). *p1* confers phlobaphene pigmentation to male and female floral organs, which is best visible in pericarp and cob glume tissue. *p1* alleles vary significantly in their tissue-specific expression patterns. For example, the *P1-rr* allele produces the reddish flavonoid pigments in both pericarp and cob glumes, whereas the *P1-wr* allele only confers

glume pigmentation (the two letter suffix after the gene designation indicates pericarp and cob color, respectively; r stands for red, w for white or colorless, and p for patterned). *P1-pr* is an epiallele of its progenitor *P1-rr*, i.e., both alleles represent different epigenetic expression states of just one nucleotide sequence (Das and Messing 1994). *P1-pr* originated from variegated kernels in a dark red *P1-rr* ear (supplemental Fig. 1). Since the pericarp tissue and the female gamete share a cell lineage, the allele resulting in a variegated phenotype may be transmissible to the next generation, namely the embryo of the patterned kernel. *P1-rr* and *P1-pr* share a complex gene structure (Fig. 1). Their coding regions are flanked by large 5.5 kb repeats that contain smaller direct repeats consisting of MULE fragments and a *p1*-specific 0.6 kb sequence. These smaller *p1*-repeats carry the distal enhancer function of *P1-rr* (Sidorenko et al. 2000). Compared to *P1-rr*, *P1-pr* is characterized by reduced *p1* transcript levels, an increased cytosine methylation level at these *p1*-repeats and permanently inaccessible chromatin structure at regulatory sequences (Lund et al. 1995).

In contrast to the paramutable alleles *B-I*, *Pl-Rh* and *R-r:std*, which change to reduced expression states rather frequently, *P1-rr* is an extremely stable allele. Only 2 in approximately 10^6 *P1-rr* kernels produced a *P1-pr* allele (Das and Messing 1994) indicating that the spontaneous silencing events of *P1-rr* are rather exceptional. Similar to the paramutant *R′* and *Pl′* alleles, *P1-pr* can be considered a metastable allele, as reversions to darker phenotypes occur repeatedly. Because *P1-pr* arises from *P1-rr* randomly and infrequently, it is not feasible to study the establishment of *P1-pr* in a homozygous *P1-rr* background. However, it is possible to investigate whether *P1-pr* is able to induce epigenetic silencing of its progenitor *P1-rr* allele when both alleles are combined in a heterozygote. Indeed, we could demonstrate that *P1-rr* is paramutable when exposed to *P1-pr*. Pigmentation phenotypes, transcript amounts, and DNA methylation levels were characterized in F1 and progeny

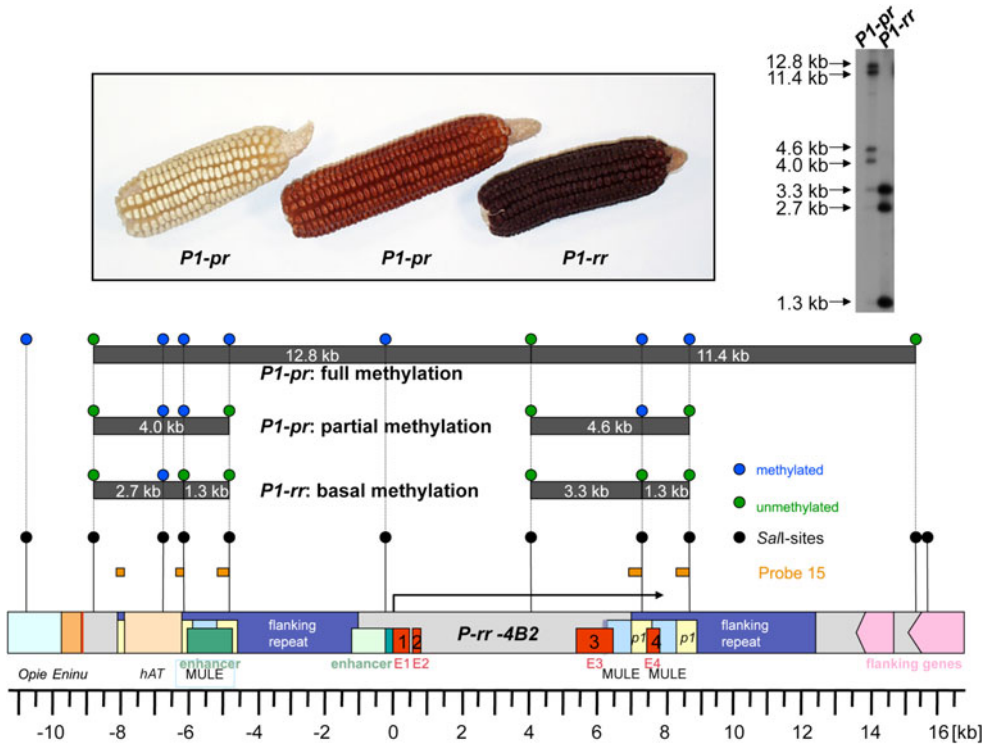

Fig. 1 Structure and cytosine methylation analysis of *P1-rr* and *P1-pr*. *P1-rr* contains 4 exons represented by *red rectangles*. The pre-mRNA is alternatively spliced such that exons 1, 2, and 3 are translated into a functional protein. The *P1-rr* coding region is bordered by 5.5-kb direct repeats (*dark blue rectangles*) that comprise smaller direct repeats, i.e., *p1*-repeats (*light yellow rectangles*) and MULE fragments (*light blue rectangles*). A *hAT*-like transposon (*tan box*) disrupts the most 5′ *p1*-repeat. Regulatory elements of *P1-rr* are drawn in *shades of green*. *Eninu* and *Opie,* two fragmented retrotransposons, are situated upstream of *P1-rr*. The 3′ end of *P1-rr* is flanked by two genes (*pink pentagons*) that are transcribed in opposite direction of *P1-rr*. A map featuring the recognition sites of the methylation-sensitive restriction enzyme *Sal*I is shown superimposed on the structure of the epi-alleles *P1-rr* and *P1-pr*. The *solid bars* above the restriction map represent *Sal*I fragments, which hybridize to probe p15. *P1-rr* (*red ear* on *top panel*) is the least methylated allele. A digest of genomic *P1-rr* DNA gives rise to two 1.3 kb bands, one 2.7 kb band and one 3.3 kb band. *P1-pr* produces a range of ear phenotypes, spanning from non-pigmented to uniformly medium-red ears (see top panel). Digests of heavily methylated *P1-pr* DNA only produce a 12.8 kb band and an 11.4 kb band. Additional bands of 4.0 kb and 4.6 kb are common for digests of less methylated *P1-pr* alleles (see Southern blot) (color figure online)

plants. We determined the cytosine methylation patterns of multiple paramutant *P1-rr′* plants with different expression patterns by bisulfite sequencing, and deduced a model for the establishment and maintenance of gene silencing based on the observed DNA methylation changes. We established that the induced gene repression of *P1-pr* constitutes a model system well suited to study establishment and subsequently maintenance and inheritance of gene silencing.

Materials and methods

Plant material

P1-rr-4B2 used for this paramutation study is a revertant derived by *Ac* excision from the *P1-vv* allele (Grotewold et al. 1991). The *P1-rr4B2* allele, which in this report is referred to as simply *P1-rr*, was introgressed in the 4Co63 inbred line and thankfully provided by Tom Peterson, Iowa State University. The epigenetically silenced *P1-pr-1 and P1-pr-2* alleles that were previously isolated in the Messing lab (Das and Messing 1994) are derived from *P1-rr-4026*. *P1-rr-4026* is a revertant that originated by *Ac* excision from *P1-ovov-1114* (Athma and Peterson 1991). In this study, we only used derivatives of the original *P1-pr-1* ear (here referred to as just *P1-pr*). *P1-pr* ears can significantly vary in phlobaphene pigmentation (Fig. 1). However, we only employed very light pigmented kernels for our genetic and molecular analysis. The *p1-ww* allele that originated in the 4Co63 background was obtained from the Maize Genetics Cooperation Stock Center (maizecoop.cropsci.uiuc.edu) collection.

Fig. 3 F1 ear phenotypes and transcript analysis. **a** F1 ear phenotypes. F1 ears vary in their pigmentation from nearly colorless to *dark red* (ears are sorted according to their pigmentation levels: the *lightest colored ear* of this representative F1 family analyzed here is shown on the *left*, while the *strongest pigmented P1-pr/P1-rr* ear is shown on the *right*. *p1-ww/P1-rr* ears do not significantly differ in their phenotypes. *Numbers* written underneath the ears identify individual F1 plants from the investigated family. Mostly half ears are shown, which are distinguished by numbers framed in *red*. The *top half* of the ear was cut 20 days after pollination and used for real-time RT-PCR analysis (see Fig. 3b). The TC and BSS labels refer to plants used for a testcross with *p1-ww* and BiSulfite Sequencing, respectively. Kernel and ear sectors are clearly noticeable in the *P1-pr/P1-rr* ears. **b** *p1* and *a1* transcript analysis of F1 ears. RNA was isolated from developing pericarp 20 days after pollination. The pericarp was derived from half ears depicted in Fig. 3a. *p1* and *a1* transcript levels were assessed by real-time RT-PCR. *p1* transcript levels were determined using an intron 2-spanning primer set. *p1* and *a1* transcript levels were normalized to actin transcript levels and calibrated to *P1-rr*, which was assigned a value of 100 %. *p1-ww* did not produce any *p1* or *a1* transcripts. *Numbers* below the *columns* refer to the F1 plants that produced the ear samples (see Fig. 3a). Data were sorted according to corresponding ear genotypes and phenotypes (from *light ears* on the *left* to *darker ears* on the *right*). Data shown represent the average of three independent real-time RT-PCRs ± standard deviation. **c** *p1* and *a1* transcription are directly proportional to phlobaphene pigmentation. Pigment amounts from F1 ears are plotted against their *p1* and *a1* transcript levels. The *plot* reveals a linear relationship between both variables. Linear regression analysis was performed on the data sets and *regression lines* are shown (color figure online)

P1-rr and *P1-pr* genotyping

The *Ac* insertion that generated *P1-ovov-1114* resulted in an 8-bp target site duplication (TSD) (see actacaac in supplemental Fig. 3). The excision of *Ac*, which gave rise to *P1-rr-4026*, left a footprint of 6 bp behind, i.e. 2 of 8 bp

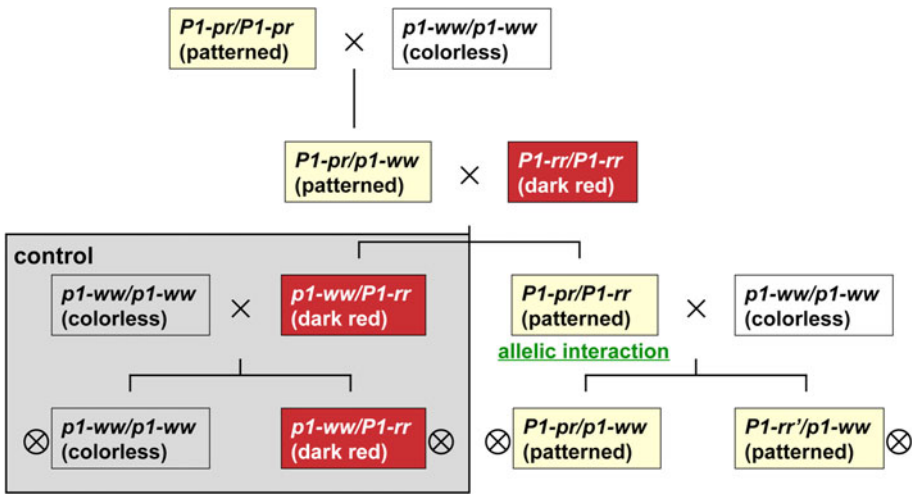

Fig. 2 Representative crossing scheme for testing paramutation at *P1-pr*. Paramutation at the *p1* locus was analyzed using the outlined crossing scheme. Homozygous *P1-pr* plants were crossed to plants carrying homozygous *p1-ww*. Subsequently, *P1-pr/p1-ww* plants were crossed to plants homozygous for *P1-rr*. An allelic interaction between *P1-pr* and *P1-rr* is made possible in this heterozygous state. Plants grown from F1 ears were testcrossed to *p1-ww* plants. As pericarp and cob glumes are maternal tissue, resulting testcross plants were self-pollinated to reveal their ear phenotype. *P1-rr* alleles that interacted with *P1-pr* are marked with a prime (′). The *colors* of the boxes containing the plant genotypes represent the corresponding ear phenotypes (color figure online)

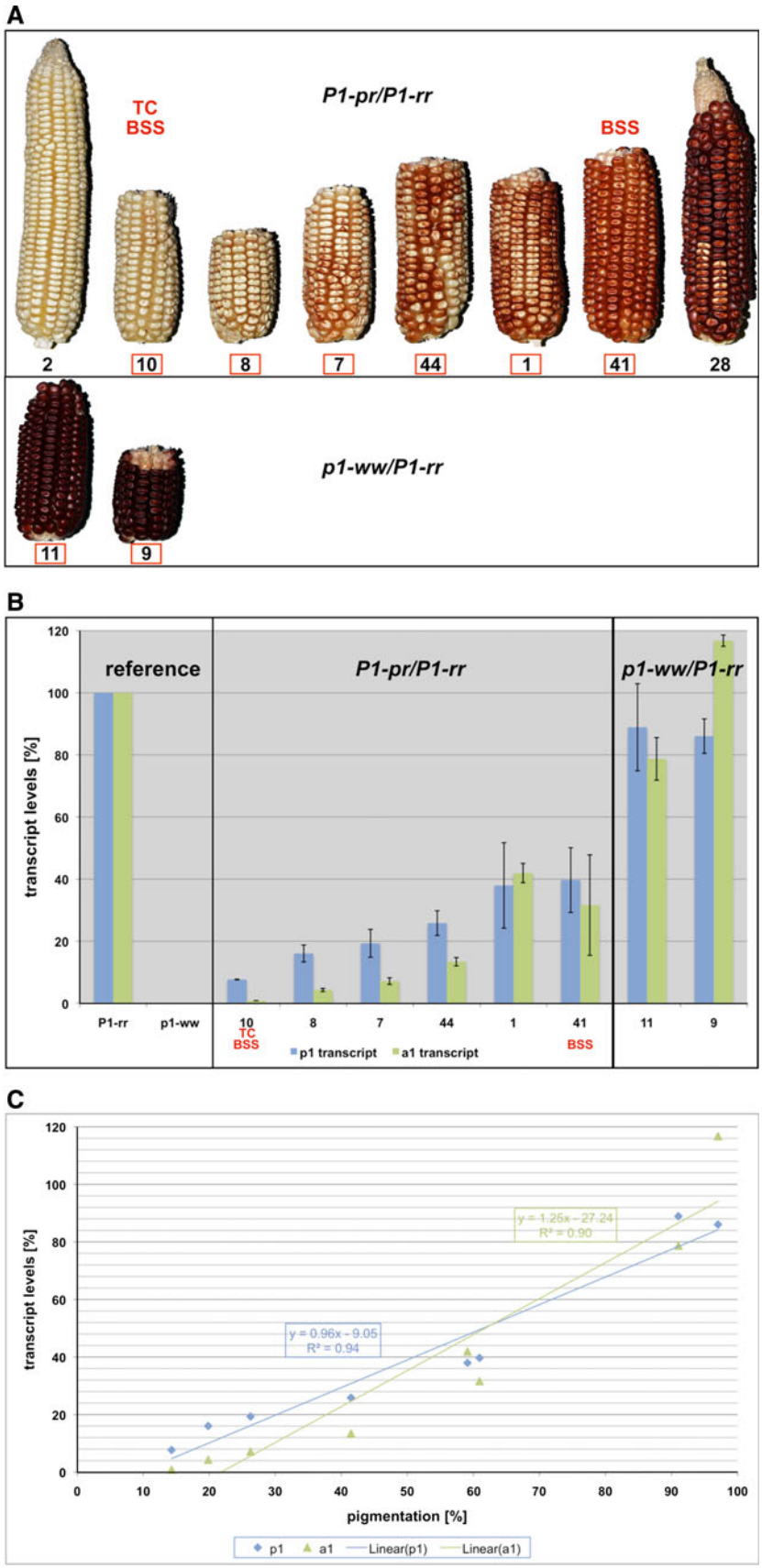
A
TC
BSS
P1-pr/P1-rr
BSS
2
10
8
7
44
1
41
28
p1-ww/P1-rr
11
9
B
reference
P1-pr/P1-rr
p1-ww/P1-rr
transcript levels [%]
P1-rr
p1-ww
10
TC
BSS
8
7
44
1
41
BSS
11
9
p1 transcript
a1 transcript
C
transcript levels [%]
y = 1.25x - 27.24
R² = 0.90
y = 0.96x - 9.05
R² = 0.94
pigmentation [%]
p1
a1
Linear(p1)
Linear(a1)

TSD were lost upon *Ac* excision. *P1-rr-4026* and, therefore, *P1-pr* contain 6 additional bp in intron 2 compared to *P1-rr-4B2* (see supplemental Fig. 3). This 6-bp indel can be used to distinguish between *P1-pr* and *P1-rr-4B2*. DNA fragments containing the indel were amplified by employing PCR primers PGT1 for 5′-TGGCGAGCTATCAAACAGGACACG-3′ and PGT1 rev 5′-GCACCGCTAGCTCTCGCAACACC-3′ that are flanking the indel. The fragments were separated on an 8 % polyacrylamide gel.

Pigment analysis

Our goal was to quantify the reddish color of maize kernels induced by the *p1* gene without destroying the samples. A chemical extraction method of phlobaphene pigments is time-consuming and renders samples useless for progeny analysis. We employed a digital camera, a consistent light source, a computer and the Adobe Photoshop graphics software (Adobe Systems Incorporated, San Jose, CA, USA) to measure and analyze the surface color of maize kernels (Yam and Papadakis 2004). Unlike special equipment or software, these tools are readily available in many laboratories. Kernels were filled in a small tray such that the bottom of the tray was completely covered. Photos were taken from the top of the tray under consistent light conditions and saved as non-compressed files (TIFF format). Files were opened with Adobe Photoshop and a section of constant size (pixel number) covering most kernels was chosen for color analysis. For each section, the average luminosity value was obtained using the Histogram Window. *p1-ww/p1-ww* and fully pigmented *P1-rr/P1-rr* kernels were assigned values of 0 and 100 %, respectively. Luminosity values within the *p1-ww* to *P1-rr* spectrum were converted in percent. Luminosity in Adobe Photoshop represents the "black-and-white" or achromatic portion of the image, which humans perceive with higher sensitivity than chromatic differences. To verify the experimental design prior to the actual measurements, *P1-rr* and *p1-ww* seeds of known ratios were mixed and their luminosity values were determined. These standard ratios were plotted against their luminosity values, which revealed the expected linear relationship. Linear regression analysis was carried out and a $R^2 = 0.99$ value supports the novel color measurement method.

RT-PCR

Total RNA was isolated from pericarp tissue 20 days after pollination with the RNeasy Plant Mini Kit (Qiagen). RNA was reverse-transcribed to cDNA using the SuperScript® III First-Strand Synthesis System (Invitrogen) with oligo(dT) and random hexamers primers. Real-time PCR amplifications were performed using the QuantiTect SYBR Green PCR Kit from Qiagen and the Rotor-Gene 3000 detection system from Corbett Research. PCR primers for the amplification of *p1* cDNAs, *a1* cDNAs and *actin1* cDNAs have following sequences:

p1cDNA-ex2-3 for 5′-GGAGGAAGAAGACATCATCATCAA-3′, p1cDNA-ex2-3 rev 5′-GAGGTGCGAGTTCCAGTAGTTCT-3′, a1cDNA-ex1-2 for 5′- GCGATCCCGCGAACGTTG-3′, a1cDNA-ex1-2 rev 5′- GCCCCTGATGGCGTCGTG-3′, actin1-ex3-4 for 5′-GGGATTGCCGATCGTATGAGC-3′ and actin1-ex3-4 rev 5′-GGACAATGCCCGGACCAGTTT-3′.

All real-time PCRs were carried out in triplicates and the average values and standard deviations were calculated.

Fig. 4 Cytosine methylation profile of *P1-pr/P1-rr* at the distal enhancer fragment as determined by bisulfite sequencing. **a** DNA methylation of F1 plants *P1-pr/P1-rr* (14.3 %) and *P1-pr/P1-rr* (60.9 %) is shown as *red* and *green markers/lines*, respectively. Both varied significantly in their ear pigmentation. DNA methylation was superimposed on structural elements of the region that contains *p1*-repeats and the distal enhancer element. Cytosine methylation was plotted separately for CG, CHG, and CHH sites (H = A, C or T). *p1*-repeats are drawn as *yellow rectangles*. The MULE fragment that divides both *p1*-repeats is illustrated as a *blue rectangle*. Insertion of a *hAT* element, which is represented as a tan rectangle, disrupts the first *p1*-repeat. The distal enhancer of *P1-rr* is located between the *Sal*I sites found in the *p1*-repeats. The methylation-sensitive *Sal*I restriction enzyme together with probe p15 (*purple rectangle*) has previously been used in Southern analyses to assess the methylation status of both epi-alleles (see supplemental Fig. 5A and B). Nucleotide positions marked underneath the *x* axis refer to the transcription start site. PCR fragments used for this methylation analysis are shown at the bottom of the figure. Please note that the internal sequences of both transposable elements were not amplified. **b** The average cytosine methylation levels ± standard deviation at CG, CHG and CHH (H = A, C or T) sites were calculated for the repeat elements shown in **a**. The sequence was divided into following segments: the region upstream of the first *p1*-repeat, the 5′ part of the first *p1*-repeat, the *hAT* element, the 3′ part of the first *p1*-repeat, the MULE fragment, and the second *p1*-repeat. Methylation data from *P1-pr/P1-rr* (14.3 %), *P1-pr/P1-rr* (60.9 %), *P1-rr* and *P1-pr* are represented by *green*, *red*, *blue* and *orange* columns, respectively. The average of *P1-rr* and *P1-pr* (shown as *gray columns*) was determined to simulate a *P1-rr/P1-pr* heterozygote without allelic interaction. **c** Cytosine methylation profiles for *P1-pr/P1-rr* (14.3 %) and *P1-pr/P1-rr* (60.9 %) have also been assayed at the repeat sequences adjacent to the coding region. All illustrations are in accordance with **a**. MULE fragments and *p1*-repeats are displayed as *blue* and *yellow rectangles*, respectively. Please notice that the first MULE fragment differs from the second one by an intact TIR (drawn as a *purple rectangle*). While the upstream MULE fragment is part of the 3′ UTR of exon 3 (marked by a *red bracket*), the downstream MULE element constitutes the 3′ end of exon 4 (indicated by a *red bracket*). *Numbers* at the *x* axis refer to the distance from the transcription start site. Positions of the stop codon and major polyadenylation sites of exon 3 are labeled with *red* and *orange vertical lines*, respectively. Although the distal enhancer fragment (marked by a *blue bracket*), which is delineated by the *Sal*I sites, is duplicated because of this repeat structure, it does not have enhancer function in this region. PCR-amplified sequences are shown below the CHH methylation profile. Please notice that due to the repeat structure most of the PCR fragments map to two regions (color figure online)

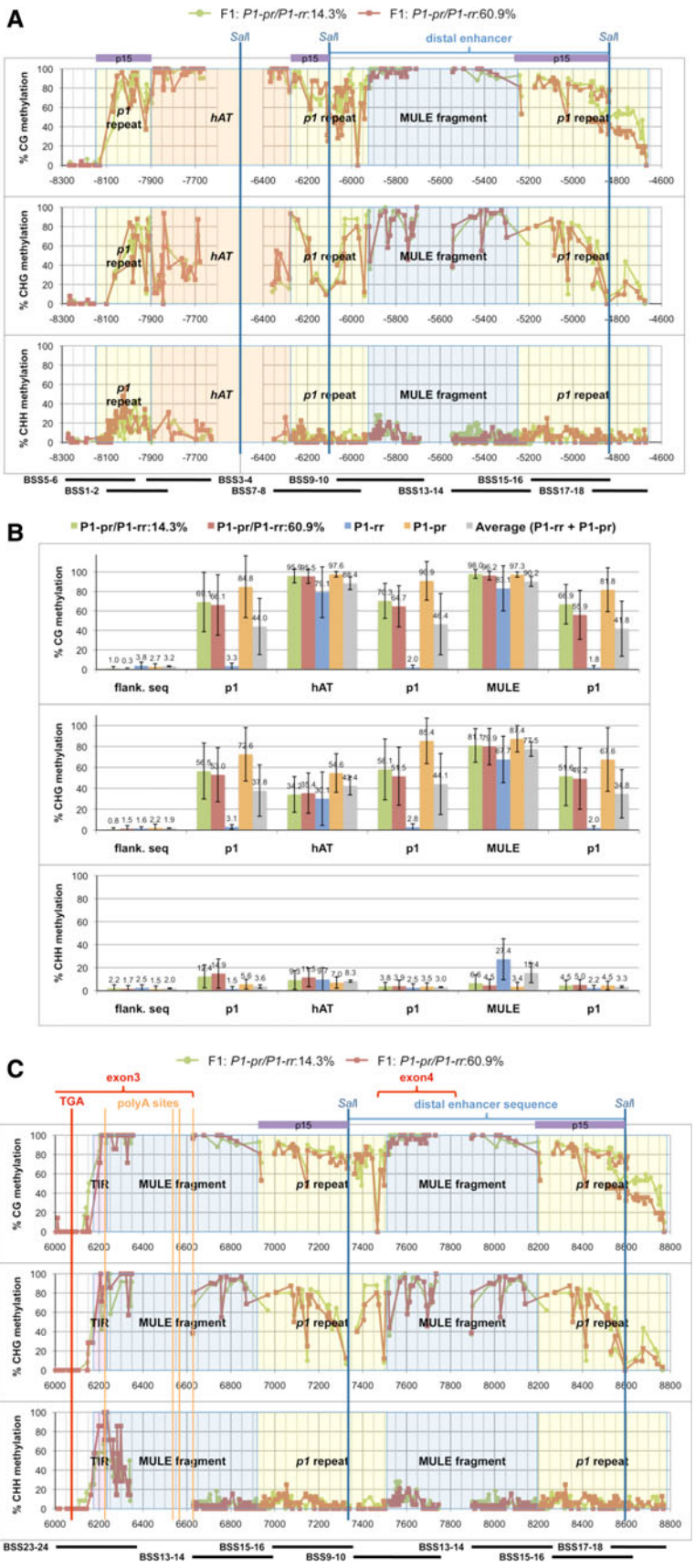
A
F1: P1-pr/P1-rr:14.3%
F1: P1-pr/P1-rr:60.9%
SalI
distal enhancer
p15
% CG methylation
% CHG methylation
% CHH methylation
p1 repeat
hAT
MULE fragment
BSS5-6
BSS1-2
BSS3-4
BSS7-8
BSS9-10
BSS13-14
BSS15-16
BSS17-18
B
P1-pr/P1-rr:14.3%
P1-pr/P1-rr:60.9%
P1-rr
P1-pr
Average (P1-rr + P1-pr)
flank. seq
p1
hAT
MULE
C
exon3
exon4
TGA
polyA sites
distal enhancer sequence
TIR
BSS23-24

Southern analysis

DNA for our Southern analysis was extracted from leaf tissue. 15 µg genomic DNA was digested with the methylation-sensitive restriction enzymes *Sal*I. Digested DNA was resolved on 0.8 % agarose gels and subsequently transferred on Amersham Hybond™-XL nylon membranes. Probe p15 (see Figs. 1, 4a, c) was labeled with ^{32}P-dCTP using the Ready-To-Go™ DNA Labeling Beads (-dCTP) from Amersham Biosciences.

Bisulfite sequencing

Genomic DNA was isolated from leaf tissue. DNA samples were subjected to sodium bisulfite treatment employing the EpiTect® Bisulfite Kit from Qiagen. The converted DNA was PCR-amplified using primers that were designed with the Methyl Primer Express® Software v1.0 from Applied Biosystems (see Table 1). Primers are based on the converted sense strand. PCR products were cloned into the pGEM®-T Easy Vector system from Promega, and 32 clones per PCR were sequenced on the 3730xl capillary sequencer (Applied BioSystems). The sequences were aligned and analyzed with the Lasergene software (DNAstar).

Results

P1-rr loses its dominance in the presence of *P1-pr*

P1-pr/P1-pr plants were crossed to plants carrying *p1-ww/p1-ww*, a null allele, which is missing the entire coding sequence and certain regulatory sequences (Goettel and Messing 2010). The *p1-ww* allele was not expected to participate in paramutation due to the truncated regulatory sequences. Heterozygous *P1-pr/p1-ww* plants were crossed to homozygous *P1-rr* plants (Fig. 2), thereby combining a silenced *P1-pr* allele with an active *P1-rr* allele in a heterozygote. *P1-pr/P1-rr* plants gave rise to ears that phenotypically ranged from *p1-ww*-like ears (without any noticeable pigmentation in pericarp and cob) to dark red ears (resembling *P1-rr* ears in pericarp and cob pigmentation) (Fig. 3a; supplemental Fig. 2). Hence, the *P1-rr* allele, which is usually dominant over alleles producing less pigment, became silenced upon exposure to *P1-pr*. However, the observed silencing effects were not uniform, instead, *P1-rr* repression appeared to occur with various intensities.

The sibling *P1-rr/p1-ww* plants consistently produced dark red ears (Fig. 3a; supplemental Fig. 2), indicating that the silencing effect segregates with *P1-pr*. Thus, *P1-rr* that never interacted with *P1-pr* in a heterozygote did not change its expression state. The outcome of reciprocal F1 crosses was indistinguishable, thereby excluding a maternal or paternal effect on *P1-rr* silencing.

F1 transcript levels

It has previously been shown (Das and Messing 1994) that phlobaphene pigment accumulation in *P1-pr* plants is tightly associated with *p1* and *a1* transcript levels. *a1* is a structural gene in the anthocyanin biosynthesis pathway, which is activated by P1. Half ears derived from *P1-pr/P1-rr* and *p1-ww/P1-rr* plants were harvested 20 DAP, at a stage where *p1* was heavily expressed in pericarp and cob glumes. However, the final ear phenotype was not established and could not be predicted at that point in development. Therefore, the selection of ears occurred in a rather random fashion. RNA for transcript analysis was isolated from kernel pericarp. *p1* and *a1* transcript levels were assessed using real-time RT-PCR. *p1* and *a1* transcripts were normalized with actin transcripts and compared to a *P1-rr* standard. Real-time RT-PCR experiments showed that *p1* and *a1* transcript levels correlated well with phlobaphene pigmentation (data are always sorted according to genotype and ear pigmentation level from light (left) to dark (right)) (Fig. 3a, b; supplemental Fig. 2). Pigment amounts plotted against *p1* and *a1* transcript levels suggested a linear relationship, which was supported by the performed regression analysis (Fig. 3c). This implied that *p1* transcript levels are also linked with *a1* transcript levels, validating the dependence of *a1* expression on *p1* expression. Compared to *P1-rr*, *p1* transcript levels ranged from about 8 to 40 % in the selected *P1-pr/P1-rr* heterozygotes, whereas corresponding ear pigmentation varied from 14 to 61 %.

To investigate whether *P1-pr*, *P1-rr* or both alleles are expressed in the F1 heterozygote, we took advantage of two features. Previously, Northern blot analysis of *p1* RNA had shown that *p1* transcripts were not efficiently spliced (Das and Messing 1994). Furthermore, a 6-bp footprint sequence present in intron 2 of *P1-pr* but not in *P1-rr* was left behind upon *Ac* excision from the progenitor allele of *P1-pr* (supplemental Fig. 3). RT-PCR of unspliced *p1* transcripts utilizing primers spanning the footprint sequence generated differently sized fragments, which could be resolved in a polyacrylamide gel. The lack of a *P1-pr* derived band suggested that *P1-pr* remained silenced in even intensely pigmented heterozygotes (supplemental Fig. 4). Accordingly, various *p1* transcript levels in F1 plants were exclusively attributed to *P1-rr* and its different epigenetic states.

F1 cytosine methylation analysis

In a separate study, we already established with bisulfite sequencing that *P1-pr* is hypermethylated compared to

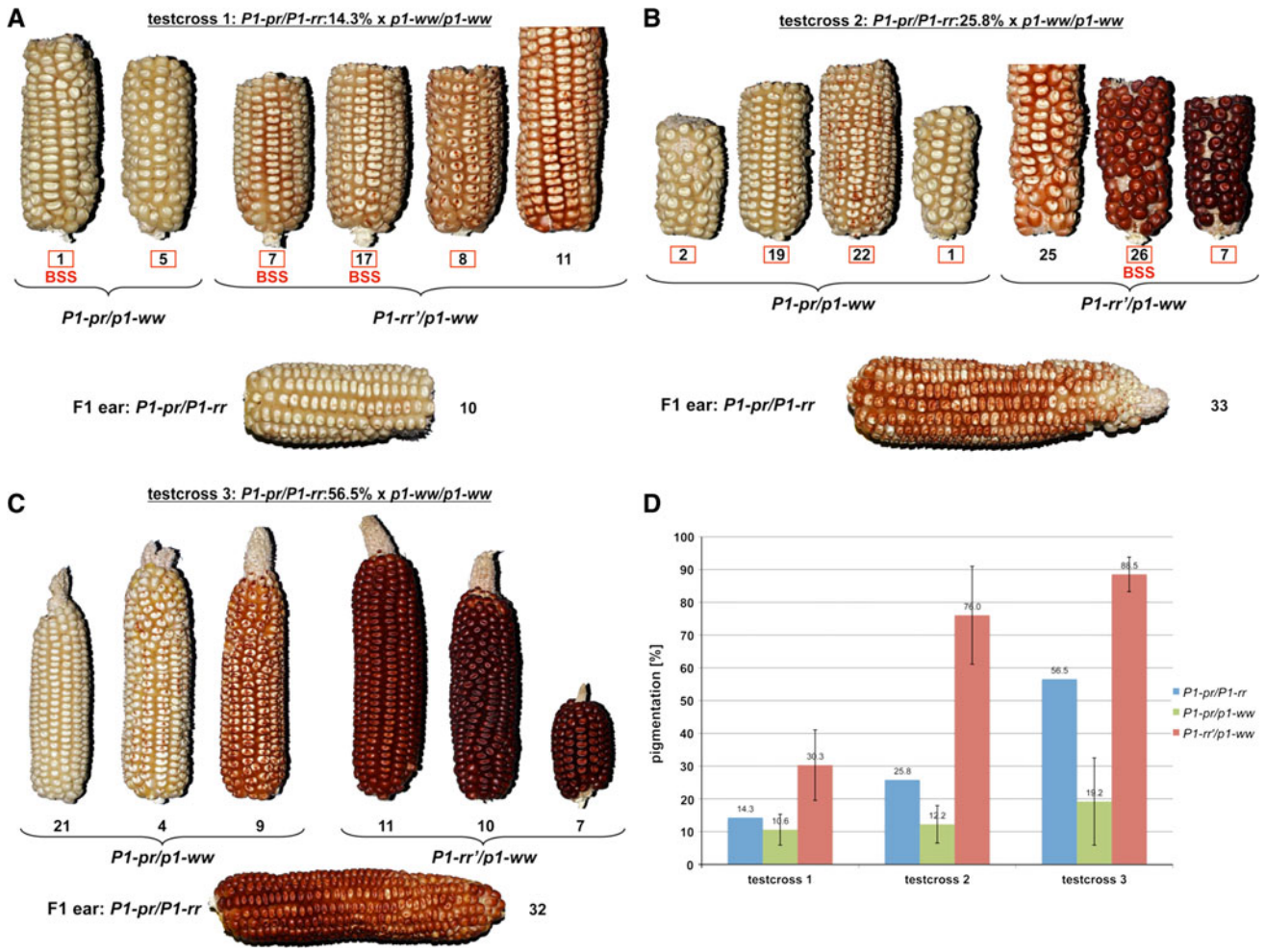

Fig. 5 Ears derived from three representative testcrosses. Ears that originated from three representative testcross families are displayed. The testcross families are derived from F1 plants *P1-pr/P1-rr* (14.3 %) (**a**), *P1-pr/P1-rr* (25.8 %) (**b**), and *P1-pr/P1-rr* (56.5 %) (**c**), which were crossed to a *p1-ww* tester. Testcross ears are sorted according to their phenotype and genotype. The lightest, the darkest and intermediate paramutant *P1-rr′* ears from the testcross families are shown. *Red frames* enclosing the plant number indicate half ears that were used for *p1* transcript analysis (see Fig. 6). BSS-labeled plants were analyzed by bisulfite sequencing (Figs. 7, 8). The progenitor F1 ear is shown at the *bottom*. The pigmentation quantity of the progenitor F1 (*P1-pr/P1-rr*) ears and the average pigmentation quantity of their corresponding testcross ears are shown in **d**. The testcross ears are grouped by *P1-pr/p1-ww* and *P1-rr′/p1-ww* genotype. Ear pigmentation levels of F1 (*P1-pr/P1-rr*) and testcross (*P1-rr′/p1-ww*) ears are correlated (color figure online)

P1-rr at the *p1*-repeats flanking the *hAT* and MULE transposons upstream and downstream of the *p1* coding region (Goettel and Messing, manuscript in preparation). The distal enhancer element was mapped to this upstream region which, therefore, could explain the gene silencing observed at *P1-pr* assuming that increased cytosine methylation inhibits proper enhancer function. To investigate paramutagenicity of *P1-pr*, we asked whether F1 plants are also associated with a change in DNA methylation of *P1-rr*. Southern blot analyses revealed that despite large differences among F1 plants regarding pigmentation and transcript levels in pericarp, the hybridization patterns of F1 plants were nearly identical (see supplement and supplemental Figs. 5A and B). To verify and to extend the results obtained by Southern blots, which only monitor few cytosine sites, we performed bisulfite sequencing on two selected F1 samples. F1 Plant #10 (*P1-pr/P1-rr*: 14.3 %) gave rise to a lightly pigmented ear, whereas F1 plant #41 (*P1-pr/P1-rr*: 60.9 %) produced a darker ear (Fig. 3a; supplemental Fig. 2). Henceforth, we will mostly use the genotype and pigmentation level in percent to designate a plant in this report. DNA extracted from leaf tissue was used for the bisulfite conversion. Comparable with the Southern blot data, both F1 plants showed a very similar DNA methylation pattern in CG, CHG and CHH contexts (Fig. 4a, b). Both were heavily methylated at the *hAT* and MULE transposons as described for *P1-rr* and *P1-pr*. Methylation at the *p1*-repeats was increased compared to *P1-rr*, but did not reach *P1-pr* levels at CG and CHG sites (Fig. 4b). Flanking sequences upstream of the 5′ *p1*-repeat

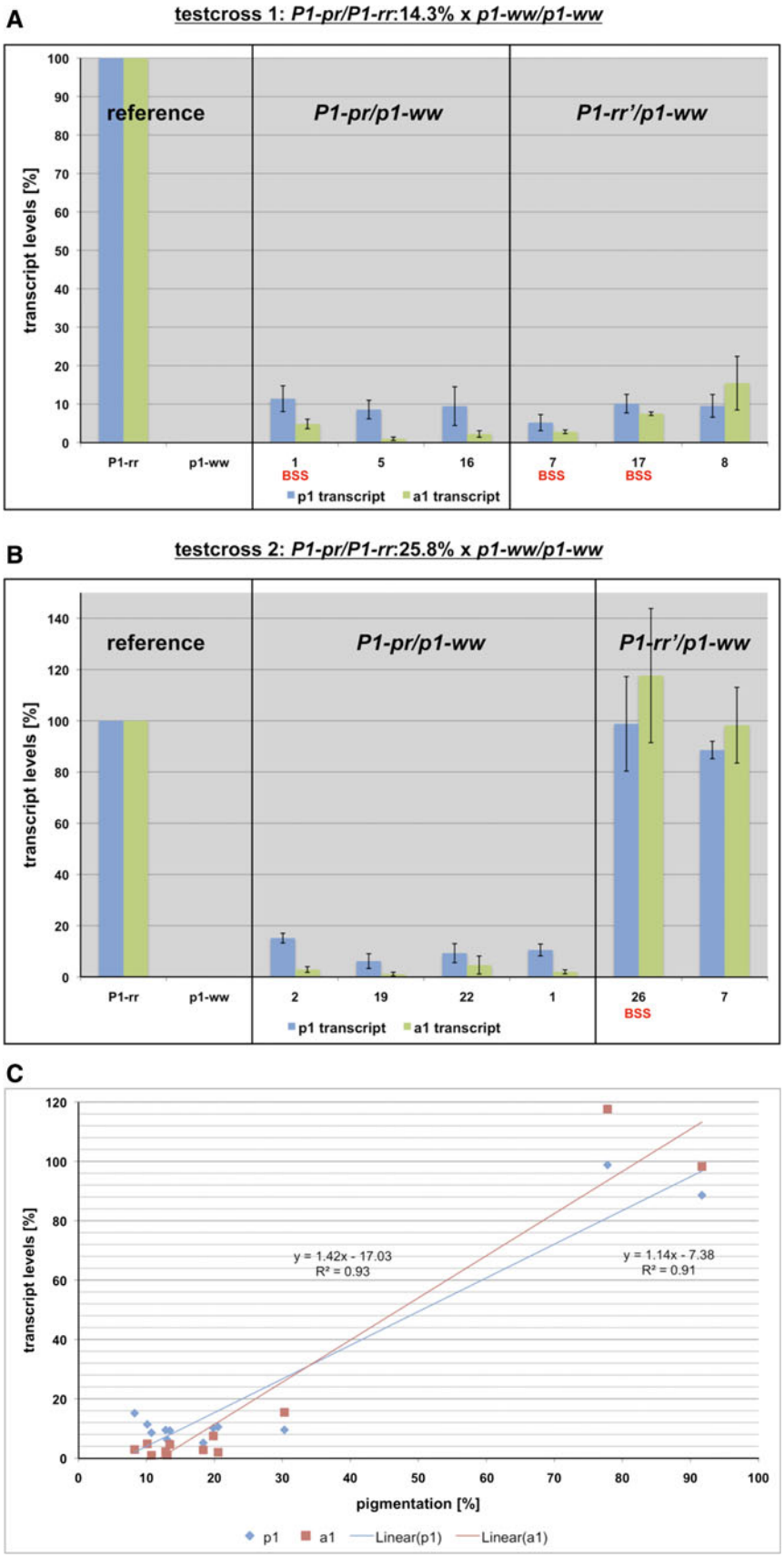

Fig. 6 *p1* and *a1* transcript analysis of ears derived from two testcrosses. Half ears for transcript analysis were chosen from two testcross families (see Fig. 5a, b). RNA was extracted from developing pericarp 20 days after pollination. *p1* and *a1* transcript levels were determined by real-time RT-PCR. *p1* and *a1* transcript levels were normalized to actin transcript levels and calibrated to *P1-rr*, which was fixed at 100 %. *p1* or *a1* transcripts were not detected for the *p1-ww* null allele. Transcript data for testcross 1 (**a**) and testcross 2 (**b**) ears were arranged by genotypes and resulting ear phenotypes. The average of three independent real-time RT-PCRs ± standard deviation is shown for each sample. BSS marks plants used for bisulfite sequencing. Pigment quantities from testcross ears are plotted against their *p1* and *a1* transcript levels (**c**). Linear regression analysis was performed on the data sets and regression lines are shown. Phlobaphene pigmentation is directly proportional to *p1* and *a1* transcript levels in testcross ears

were unmethylated. Despite a 4.3-fold and 5.1-fold difference in pigment and transcript levels between the F1 plants *P1-pr/P1-rr* (14.3 %) and *P1-pr/P1-rr* (60.9 %), respectively, the plant producing the darker ear was on average only 7 % less methylated at CG sites in all *p1* repeats than the plant with the lighter ear.

Figure 4a represented the DNA methylation level of an F1 plant in one graph, although each allele of the *P1-pr/P1-rr* heterozygote could have a distinct methylation pattern as they maintained or altered their original DNA methylation separately. Accordingly, a methylation change in the F1 plants had to be measured as the deviation from the average cytosine methylation of the parental *P1-rr* and *P1-pr* alleles (Fig. 4b). Compared to this average, CG methylation at *p1*-repeats of F1 plants *P1-pr/P1-rr* (14.3 %) and *P1-pr/P1-rr* (60.9 %) was increased by about 25 and 18 %, respectively. In contrast to the transcribed region, we cannot distinguish whether the sequenced PCR fragments were derived from *P1-rr* or *P1-pr* due to a lack of polymorphisms in this region. However, we could compare the methylation pattern of individual clones with that of typical *P1-rr* and *P1-pr* plants and classify their methylation pattern accordingly. We chose PCR fragments amplified with primers BSS7-8 for this analysis because they were derived from just one genomic site (Fig. 4a). Due to the repeat structure of the *P1-rr* and *P1-pr* alleles, some PCR fragments could originate from up to three genomic sequences (Fig. 4). BSS7-8 clones from *P1-rr* revealed the described CG methylation pattern, i.e., the *p1*-repeat was unmethylated and the flanking *hAT* element showed a varying amount of CG methylation (supplemental Fig. 6A). In contrast, *P1-pr* clones were highly methylated at CG sites in the *p1*-repeat and in the *hAT* transposon (supplemental Fig. 6B). 14 out of 32 BSS7-8 clones from *P1-pr/P1-rr* (14.3 %) resembled *P1-pr* in their CG methylation pattern, whereas the remaining 18 clones were more methylated than *P1-rr*, but significantly less than *P1-pr* (supplemental Fig. 6C). Most of the clones (22 out of 30) from the F1 plant *P1-pr/P1-rr* (60.9 %), which yielded a darker ear, were less methylated than *P1-pr* (supplemental Fig. 6D). The presence of two distinct groups, one identical with *P1-pr* and the other roughly resembling *P1-rr*, could indicate that a methylation change more likely happened at the *P1-rr* allele of the heterozygote because this scenario requires the least methylation changes from the parental alleles to the observed pattern in the F1. CHG methylation in BSS7-8 clones was lower than CG methylation. However, the analysis of individual clones for *P1-rr*, *P1-pr* and *F1* plants supports the above results (supplemental Figs. 6E–H).

p1-repeats downstream of the coding region revealed the same cytosine methylation pattern as reported for *P1-pr* (Fig. 4c). The overall repeat structure is similar to the *p1*-repeat arrangement at the enhancer region. While the first *p1*-repeat is not interrupted by a *hAT*-like element, the *p1* sequence is flanked at the 5′ end by an additional copy of the MULE. In summary, the huge variability of F1 ear phenotypes was clearly not reflected in the *P1-pr/P1-rr* cytosine methylation levels in the regions evaluated. Furthermore, few *P1-pr/P1-rr* ears were phenotypically indistinguishable from *P1-pr* ears, although they substantially differed in their cytosine methylation levels (for example, see ear #2 in Fig. 3a and *P1-pr/p1-ww* control in Fig. 5a). This could suggest that a change in cytosine methylation lags behind the establishment of an epigenetic expression state. In general, our bisulfite data confirmed that the *Sal*I restriction enzyme was suitable for the initial characterization of the *P1-pr* and *P1-rr′* methylation status because the restriction sites monitored with probe 15 were located in the *p1*-repeat regions that were variable for cytosine methylation.

The silenced *P1-rr′* allele is heritable

Expression of the *P1-rr* allele was reduced in the presence of a *P1-pr* allele. However, it remained to be tested whether the modified *P1-rr* allele is (1) heritable and (2) retains its pigmentation potential shown in the F1 ear phenotype. Therefore, *P1-pr/P1-rr* plants were crossed to a homozygous *p1-ww* tester (Fig. 2). Testcross plants derived from F1 plants 10, 33, and 32 (supplemental Fig. 2), which gave rise to weakly (14.3 %), intermediately (25.8 %) and strongly pigmented ears (56.5 %), respectively, were chosen for further analysis. Testcross plants were genotyped based on the presence or absence of the 6-bp footprint sequence (supplemental Fig. 3) using the above-mentioned PCR assay (data not shown).

The *P1-pr* allele emerged from most *P1-pr/P1-rr* heterozygotes phenotypically unchanged (note that testcross ear 9 shown in Fig. 5c represents a rare reversion of *P1-pr* to a higher expression state). In contrast, the original *P1-rr* phenotype was rarely recovered from heterozygotes (Fig. 5a–c), implying that the silenced *P1-rr′* allele (designated *P1-rr′* after exposure to *P1-pr*) is transmitted through meiosis. This presents a clear violation of Mendel's First Law. In all three testcrosses shown, *P1-rr′/p1-ww* ears were always more pigmented than *P1-pr/p1-ww* ears (supplemental Figs. 7A–C) indicating that *P1-rr′* silencing had not reached the *P1-pr* level. Also, *P1-rr′/p1-ww* testcross ears seemed to vary in their pigmentation and, therefore, silencing state more than *P1-pr/p1-ww* ears. F1 ear pigmentation levels (14.3, 25.8 and 56.5 %) ranked approximately between that of *P1-pr/p1-ww* and *P1-rr′/p1-ww* ears (Fig. 5d). F1 ear pigmentation correlated with testcross ear pigmentation. The darker the F1 ear the more pigmented were the *P1-rr′/p1-ww* and *P1-pr/p1-ww* testcross ears. *P1-pr/P1-rr* (14.3 %), *P1-pr/P1-rr* (25.8 %) and

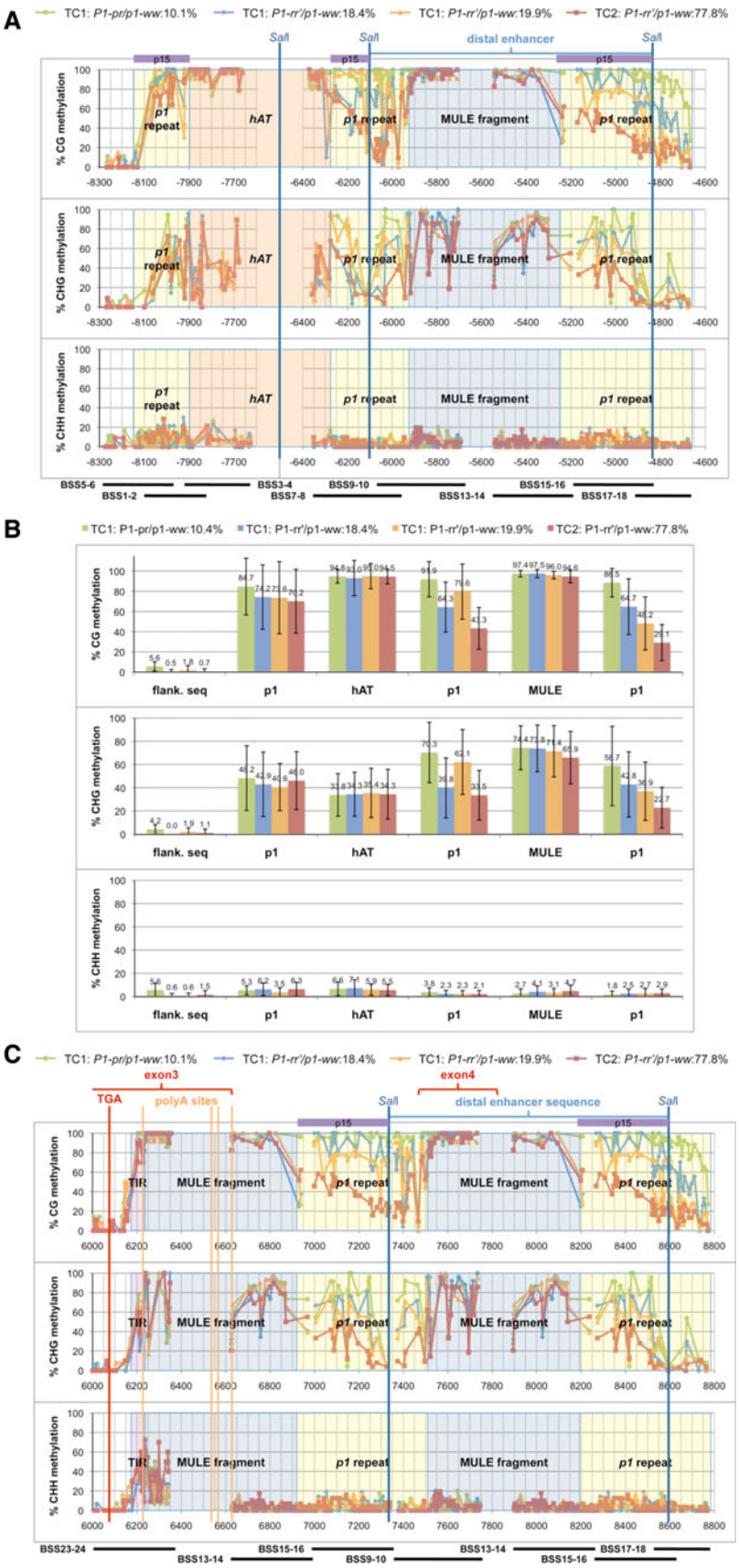

Fig. 7 Cytosine methylation profile of *P1-pr* and *P1-rr′* at the distal enhancer fragment as determined by bisulfite sequencing. DNA methylation profiles of testcross 1 plants *P1-pr/p1-ww* (10.1 %), *P1-rr′/p1-ww* (18.4 %) and *P1-rr′/p1-ww* (19.9 %) and testcross 2 plant *P1-rr′/p1-ww* (77.8 %) are plotted in *green*, *blue*, *orange* and *red*, respectively. Only *P1-pr* and *P1-rr′* alleles are shown (for *p1-ww* see Fig. 8). Identical to Fig. 4a, methylation data are superimposed on a graphical representation of the distal enhancer region (**a**) and the fragment adjacent to the coding region (**c**) that also contains the enhancer repeat. The average cytosine methylation levels per structural element as indicated in **a** were calculated for testcross plants *P1-pr/p1-ww* (10.1 %), *P1-rr′/p1-ww* (18.4 %), *P1-rr′/p1-ww* (19.9 %), and *P1-rr′/p1-ww* (77.8 %), which are presented by *green*, *blue*, *orange* and *red* columns, respectively (**b**) (color figure online)

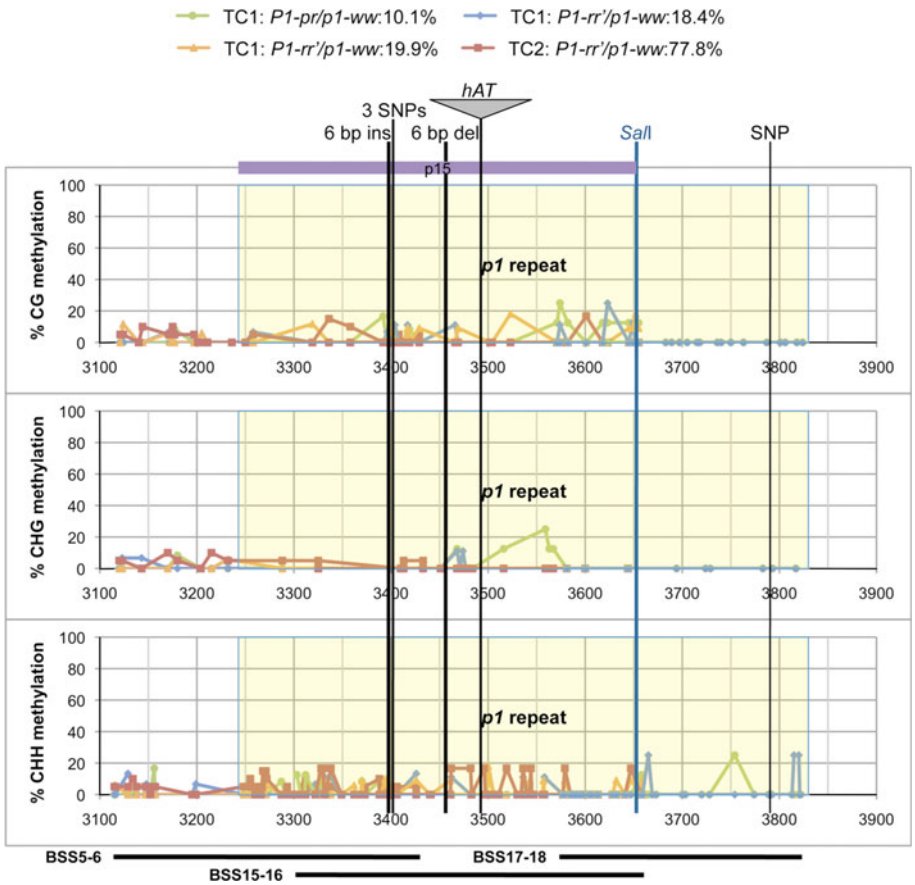

Fig. 8 Cytosine methylation profile of *p1-ww* at the *p1*-repeat as determined by bisulfite sequencing. DNA methylation levels of the heterozygous testcross plants *P1-pr/p1-ww* (10.1 %), *P1-rr′/p1-ww* (18.4 %) and *P1-rr′/p1-ww* (19.9 %) and *P1-rr′/p1-ww* (77.8 %) were assessed by bisulfite sequencing. Whereas cytosine methylation of *P1-pr* and *P1-rr′* alleles is shown in Fig. 7a, c, DNA methylation of the corresponding *p1-ww* alleles is presented in this chart. CG, CHG and CHH (H = A, C or T) methylation profiles were plotted across an annotated *p1-ww* sequence using the same sample colors and markers as in Fig. 7a, c. The *p1*-repeat (*yellow rectangle*) and its flanking regions only differ by few SNPs and indels from *P1-rr* as shown by *vertical lines*. However, *p1-ww* lacks the repeat structure and the *hAT* element. The insertion site of the *hAT* transposon in *P1-rr* is indicated for purpose of orientation. The restriction site for the methylation-sensitive enzyme *Sal*I and the location of probe p15 (*purple rectangle*), which detected a 1.1 kb band in Southern analyses in supplemental Fig. 8a–c, are shown. *Numbers* on the *x* axis refer to nucleotide position in the *p1-ww* sequence (GenBank accession number HM454274). The genomic origin of the PCR fragments used for this methylation analysis is illustrated at the base of the figure (color figure online)

P1-pr/P1-rr (56.5 %) produced ears with an average pigmentation of 30.3, 76, and 88.5 %, respectively (Fig. 5d).

Transcript analysis of testcross plants

Subsequent transcript analysis of testcross plants was performed as described above for F1 individuals. Six ears per testcross were randomly chosen and analyzed by real-time RT-PCR. As expected, *p1* and *a1* transcript levels from *P1-pr/p1-ww* plants remained low, which were consistent with the weakly pigmented ear phenotypes (Fig. 6a, b). Accordingly, *P1-pr* expression was not influenced by *P1-rr* in the heterozygotes that gave rise to testcross 1 and 2 ears. The paramutant *P1-rr′/p1-ww* plants accumulated *p1* and *a1* transcript levels ranging from *P1-pr* to *P1-rr* levels (Fig. 6a, b). *p1* and *a1* transcript levels of *P1-rr′/p1-ww* plants were generally associated with their kernel phenotypes (Fig. 6c). For example, *P1-rr′* plants that produced lightly pigmented ears such as testcross 1 samples had less *p1* and *a1* transcripts than plants that gave rise to darker ears such as testcross 2 individuals.

Cytosine methylation analysis of testcross plants

DNA methylation of testcross plants was analyzed in a similar fashion as described for F1 plants (see above). *P1-rr′* cytosine methylation levels seemed to be inversely correlated with the testcross phenotypes when we compared multiple testcross families by Southern analysis (see supplement and supplemental Fig. 8A–C). To confirm these results, we chose four testcross plants with different pigment intensities for bisulfite conversion and sequencing

of the variable region as described above. Testcross 1 plants *P1-pr/p1-ww* (10.1 %), *P1-rr′/p1-ww* (18.4 %) and *P1-rr′/p1-ww* (19.9 %) were derived from the *P1-pr/P1-rr* (14.3 %) ear and testcross 2 plant *P1-rr′/p1-ww* (77.8 %) originated from *P1-pr/P1-rr* (25.8 %). As seen for *P1-rr* and *P1-pr* and for *P1-pr/P1-rr* (Fig. 4a–c), both *hAT* and MULE transposons were highly and consistently methylated in all tested samples (Fig. 7a, b). In contrast, DNA methylation at *p1*-repeats varied in each investigated plant. The average methylation of all cytosines within *p1*-repeats was inversely correlated with the ear phenotype of the corresponding plant (supplemental Fig. 9). The highest methylated *P1-rr′* allele (67.7 % at CG sites) gave rise to the least pigmented *P1-rr′/p1-ww* (18.4 %) ear while the lowest methylated *P1-rr′* allele (47.5 % at CG sites) produced the most pigmented *P1-rr′/p1-ww* (77.8 %) ear. Importantly, *p1* methylation differed in each repeat. The upstream part of the *p1*-repeat, which is interrupted by the *hAT* element, showed very little variation in methylation among tested plants compared to the remaining downstream sequence and the second *p1*-repeat (Fig. 7b). The distal enhancer element is located in *p1* sequences that revealed more diverse methylation patterns (Fig. 7a). In addition, methylated cytosines were not evenly distributed within *p1*-repeats. CG and CHG methylation decreased as a function of distance from the MULE and *hAT* transposons, and the drop in methylation was more pronounced for less pigmented plants. Most curiously, DNA methylation did not exceed the 5′ or 3′ end of both *p1* repeat sequences.

Cytosine methylation at the *p1*-repeats and MULE transposons downstream of the coding region mirrored that of the identical sequences 4.6 kb upstream of the transcription start site. Interestingly, the only significant amount of CHH methylation measured in both regions was at the 5′ end of the MULE that is part of exon 3 (Fig. 7c). The average CHH methylation across this 5′ terminus was 29.9, 26.2, 29.9 and 36.4 % for *P1-pr/p1-ww* (10.1 %), *P1-rr′/p1-ww* (18.4 %), *P1-rr′/p1-ww* (19.9 %) and *P1-rr′/p1-ww* (77.8 %), respectively.

The paramutationally neutral *p1-ww*[4Co63] allele is not methylated

In our crossing scheme, we used the *p1-ww*[4Co63] allele as a tester which in turn also becomes heterozygous with *P1-pr* or *P1-rr′* (Fig. 2). *p1-ww*[4Co63] is a null allele that is missing the complete coding region and some regulatory sequences (Goettel and Messing 2010). Nevertheless, *p1-ww* contains a *p1*-repeat that only varies in two SNPs and four small indels from that of *P1-rr* or *P1-pr*. Interestingly, the *p1-ww* allele remains unmethylated at *Sal*I sites in every testcross plant as can be seen in the uniform 1.1 kb bands in our Southern blots (supplemental Fig. 8A–C). We also determined by bisulfite sequencing the DNA methylation pattern of a 710 bp region that includes the *p1-ww p1*-repeat. Our results for this sequence show that *p1-ww* when heterozygous with *P1-pr* or *P1-rr′* is devoid of DNA methylation in all cytosine contexts (Fig. 8). The *p1-ww*[4Co63] allele apparently does not interact with *P1-pr* or *P1-rr′*, which renders it a neutral allele in terms of paramutation indeed suitable for testcrosses (Sidorenko and Peterson 2001).

Taken together, the testcross analysis established that *P1-pr* is a paramutagenic allele, while *P1-rr* is a paramutable allele. The paramutant *P1-rr′* allele resembles *P1-pr,* although *P1-rr′* is less silenced compared to the inducing *P1-pr* allele. Similar to *P1-pr*, *P1-rr′* is able to heritably silence a naïve *P1-rr* allele in a heterozygote, but *P1-rr′* is less paramutagenic than *P1-pr* (data not shown). *p1-ww* did not participate in *p1* paramutation, which identifies *p1-ww* as a neutral allele.

Discussion

Genetic characterization

P1-rr is usually dominant over *p1* alleles that confer less phlobaphene pigmentation to plant tissues. However, when *P1-rr* is combined with *P1-pr* in a heterozygote, *P1-rr* can lose its dominance. *P1-pr/P1-rr* ears can display a wide variety of phenotypes, ranging from *P1-rr* to *P1-pr* pigmented ears. The parental *P1-rr* expression profile of full pigmentation is never recovered from a weakly pigmented heterozygote in an F2 or testcross generation, suggesting that *P1-rr* changed to a *P1-pr* expression state, which can be transmitted through meiosis. *P1-rr′* is also able to paramutate naïve *P1-rr* alleles that previously have never interacted with *P1-pr* (data not shown). Although *P1-rr′* acquires paramutagenicity, its paramutagenic strength is reduced compared to the initial silencing by *P1-pr*. The non-functional *p1-ww* allele lacks the potential to acquire paramutagenicity after exposure to *P1-pr*, which renders *p1-ww* neutral with respect to *p1* paramutation.

Cytosine methylation follows the establishment of *P1-pr* silencing

Although *P1-rr* and *P1-pr* share an identical sequence, the epialleles are differentially methylated at CG, CHG and CHH sites, as monitored by methylation-sensitive restriction enzymes and bisulfite sequencing. Phenotype and transcript levels are inversely correlated with the cytosine methylation pattern such that a reduction in pigmentation is reflected in an increased methylation (Das and Messing 1994). In contrast, the methylation state is not predictive

for pigmentation in F1 plants. *P1-pr/P1-rr* plants revealed that the change of cytosine methylation seemed to lag behind the establishment of the silenced epigenetic state. Vice versa, *P1-pr* plants that revert to full color either spontaneously or due to the effects of the epigenetic modifier *Ufo1* (Chopra et al. 2003) still show increased methylation levels, suggesting that a decrease in methylation follows gene reactivation (Das and Messing 1994). However, once gene silencing is established, DNA methylation of the meiotically transmitted *P1-rr′* allele is again associated with its gene expression. In testcross plants, methylation levels of paramutant *P1-rr′* alleles vary according to pigmentation levels. Although methylation levels and phenotypes never reached *P1-pr* levels the major alterations of methylation also occurred within the *p1*-repeats that contain the distal enhancer region. Similar to *P1-rr′*, a methylation change during paramutation has been reported for the paramutant *B′* (Haring et al. 2010) and *R-r:std* (Walker 1998) alleles (see below).

cis-Requirements and transgene silencing

Epigenetic silencing of an endogenous *P1-rr* allele has been observed previously. A transgene that contained the 1.2-kb *P1-rr* distal enhancer fragment driving a GUS reporter gene was able to change a *P1-rr* allele into a *P1-pr* expression state (Sidorenko and Chandler 2008; Sidorenko and Peterson 2001). Not surprisingly, the GUS transgene was co-silenced. Constructs carrying the proximal enhancer did not cause suppression of the endogenous *P1-rr* gene, suggesting that the 1.2-kb distal enhancer fragment is necessary and sufficient to inactivate the homologous *P1-rr* allele. The transcriptionally silenced paramutant-like state, named *P1-rr′*, was heritable even in absence of the inducing transgene (Sidorenko and Chandler 2008; Sidorenko and Peterson 2001). Identical to the naturally derived *P1-pr*, the transgene-induced *P1-rr′* was paramutagenic, revealing indistinguishable behavior in genetic crosses. The transgenes were present in approximately 5–15 copies, indicating that larger quantities of the distal enhancer may increase the probability for spontaneous silencing of the typically very stable *P1-rr* allele.

Transposon silencing and paramutation at *p1* appear to be linked

Diverse silencing phenomena, such as transposon cycling, paramutation and transgene silencing, have been found to be mechanistically linked. For example, the *mop1-1* mutation has been shown to reactivate several (but not all) paramutant alleles (Dorweiler et al. 2000), a transposable element (but not all) (Lisch et al. 2002), and several transgenes (McGinnis et al. 2006). Our proposed model for spontaneous and induced *P1-pr* silencing also connects the control of transposable elements with paramutation. A model capable of explaining *P1-pr* paramutation has to take into account several features: (1) Silencing in the F1 generation can vary in a rather random fashion. (2) *P1-pr* in a F1 heterozygote remains silenced as evidenced by sustained methylation and transcript levels. (3) Silencing in F1 and DNA methylation are not associated. (4) Silencing of the paramutant *P1-rr′* negatively correlates with DNA methylation. (5) Although not tested here, a chromatin change is likely for *P1-rr′* based on data of the paramutagenic *P1-pr* allele (Lund et al. 1995). (6) Homologs of the Arabidopsis RdDM pathway are involved in *p1* silencing (Sidorenko and Chandler 2008; Sidorenko et al. 2009).

RNA-directed DNA methylation (RdDM) is best understood in Arabidopsis where repeat sequences, endogenous genes and transgenes are methylated as a consequence of this pathway (Haag and Pikaard 2011). RdDM in maize and Arabidopsis probably is mechanistically similar, however, siRNA analysis in *mop1* mutant plants indicates additional mechanisms in maize for the production of heterochromatic siRNAs (Nobuta et al. 2008). A current but simplified model for RdDM in Arabidopsis is outlined here (Haag and Pikaard 2011). The silencing pathway begins with a sequence that is transcribed by Pol IV. Pol IV noncoding transcripts are copied into double-stranded RNA (dsRNA) by the RNA-DEPENDENT RNA POLYMERASE2 (RDR2). The dsRNA is diced by DICER-LIKE3 (DCL3) into 24 nt duplexes. siRNAs are being stabilized by HUA-ENHANCER1 (HEN1) that adds a methyl group to their 3′ ends. A single strand of the duplex is loaded onto ARGONAUTE4 (AGO4) and assembled into the RNA-induced silencing complex (RISC). Pol V provides RISC with a target because AGO4 interacts with Pol V or Pol V noncoding transcripts via base-pairing of the siRNAs. AGO4 recruits chromatin-modifying enzymes and the de novo cytosine methyltransferase DOMAINS REARRANGED METHYLTRANSFERASE 2 (DRM2) to Pol V transcribed loci, which undergo histone modifications and DNA methylation. AGO4 can also slice Pol V transcripts that in turn can be copied by RDR2 and used for secondary siRNAs production.

Here, we propose a multi-step model starting from the establishment of *P1-pr* silencing to the maintenance of the repressed paramutant *P1-rr′*. The first step leads to a chromatin change at the MULE fragments in *P1-rr*. A putative full-length MULE or deletion derivative somewhere in the genome is transcribed and produces 24 nt siRNAs. These siRNAs are used in RISC to target the transcribed locus of origin and other homologous sequences for chromatin and methylation change. Although the MULE transposons in *P1-rr* are very fragmented, they are sufficient to act as targets for the siRNAs produced in trans. This interaction

results in a change of the epigenetic state at the *P1-rr* transposon fragments, which is reflected in the increased CHH methylation of *P1-rr* compared to *P1-pr* at these sites. Possibly, the MULE fragment 3′ of the coding region, which has a complete 5′ TIR, plays a role in this initial interaction as *P1-pr* is methylated in this TIR whereas *P1-rr* is not. An epigenetic change of the *P1-rr* MULE transposons might also be achieved by transgenic constructs that carry the MULE fragment and flanking sequences (Sidorenko and Chandler 2008; Sidorenko and Peterson 2001). Random insertions in the genome allow the production of aberrant transcripts, which can be the source of 24 nt siRNAs that are fed into the RdDM pathway. Thereby they could also target the MULE fragments in *P1-rr*.

The second step involves the establishment and maintenance of the *P1-pr* epigenetic state, which could be caused by spreading of DNA methylation from the transposon fragments into flanking sequences. The above-mentioned RdDM model suggests that Pol IV transcripts stemming from transposons are mostly terminated at the transposon borders. However, Pol V might transcribe also adjacent euchromatic sequences far beyond the transposons. In case of *P1-rr*, Pol V transcripts could be terminated in the *p1* repeats or even in the adjacent transposon, which in the later case would explain why the maximum length of the methylated region coincides with the repeat unit. RDR2 copies the extended transcripts into dsRNAs, which are sliced by DCL3 into 24 nt secondary siRNAs. The siRNAs guide the RISC machinery to the complementary scaffold RNA and recruits enzyme complexes for cytosine methylation and chromatin modifications. The *P1-rr* distal enhancer is accidentally packaged in condensed chromatin, which prevents the enhancer from interacting with the promoter by, for example, a long-range looping mechanism as proposed for *B-I* and *B′* (Louwers et al. 2009). Therefore, the elongated Pol V transcripts result in an epigenetic change from *P1-rr* to *P-pr*. The novel heterochromatic region is stabilized by maintenance methylation at CG and CHG sites. At this stage, only the TIR of the MULE in exon 3 has a significant CHH methylation and, therefore, might be transcribed for siRNA production.

The third step is concerned with the allelic crosstalk between *P1-pr* and *P1-rr* in a heterozygote. siRNAs are being produced from the MULE TIR of the *P1-pr* allele. Some of the siRNAs bound to RISC diffuse to the *P1-rr* allele, which has a different epigenetic state than *P1-pr*. Similar to the spontaneous event that generated *P1-pr*, siRNAs initially only change the epigenetic state of the transposon targets, which then in turn allows transcription by Pol V into flanking sequences. As described above, the Pol V transcripts result in chromatin and methylation changes across the length of the transcripts. These Pol V transcripts can be of variable length. Shorter ones might not reach the enhancer element and consequently do not cause *P1-rr* silencing, whereas longer transcripts cover the entire enhancer region and drastically reduce gene expression. These stochastic events are independent of *P1-pr* as can be seen in F1 ears ranging from lightly to fully pigmented. If siRNAs produced from the *P1-pr* allele were to determine the methylation pattern of both *P1-pr* and *P1-rr* alleles in a heterozygote, DNA methylation of both alleles should be identical because chances of finding *P1-pr* or *P1-rr* and implementing the methylation change should be the same. In addition, having two instead of just one target sequence would dilute the available siRNAs per sequence, possibly losing its silencing efficiency if the siRNA amount drops below a certain threshold level. However, this is not the case.

This model is also applicable to the lack of interaction between *P1-pr* and *p1-ww*. *P1-pr* does not seem to have any effect on DNA methylation of *p1-ww*. Since *p1-ww* is missing the MULE and *hAT* transposons, scaffold transcripts cannot be initiated that could bind the RISC machinery causing methylation and chromatin modifications.

In summary, this model assumes that the required regions for the allelic crosstalk are within the transposons because this is from where the transcripts and, therefore, silencing originate. The adjacent enhancer is the actual sequence necessary for silencing, and gene repression is mediated by chromatin modification followed by cytosine methylation. This model also accounts for the observation that the spontaneous silencing of epialleles is inbred line dependent (Walbot 2001), because inbred lines can substantially vary in their transposon composition (Du et al. 2011) and accordingly availability of silencing triggers.

Silencing of *R-r:std* is also associated with a transposable element

A putative link between transposable elements and paramutation has been reported previously (Martienssen 1996; Walker 1998). Paramutation of *P1-rr* resembles silencing of the highly complex *R-r:std* allele in structure and function. *R-r:std* consists of four partial and intact genes, two of which are sensitive to paramutation, namely *S1* and *S2*. The complete genes *S1* and *S2* are arranged in an inverted head-to-head orientation and are separated by a fragmented *doppia* transposable element of 387 bp that functions as a promoter for both genes. The paramutant *S1* and *S2* alleles show an increase in cytosine methylation in the sequences flanking doppia whereas the active alleles are unmethylated (Walker 1998). Interestingly, a spontaneous deletion derivative that lacks almost the entire *doppia* element is transcription and methylation deficient suggesting that this *doppia* sequence is possibly required for paramutation at *R-r:std*. The repeat structure of *R-r:std*

Table 1 List of PCR primers used to amplify bisulfite-treated *P1-pr* and *P1-rr* DNA

Name	Primer sequence	Orientation
BSS1	5′ TTTATGTGGTTTGTTGTTTGT 3′	for
BSS2	5′ AAAAAAAAACCRATAATTAACC 3′	rev
BSS3	5′ TGGTTAAATAATTGTAGGGAGA 3′	for
BSS4	5′ TACRAATTTCATCTTCACATATAA 3′	rev
BSS5	5′ TTATGTTGTTTGTTAGTYGATTT 3′	for
BSS6	5′ TCCCTACAATTATTTAACCATCT 3′	rev
BSS7	5′ AAATGATTTGGTTTGGTTAAAT 3′	for
BSS8	5′ TCAAATAACRCCTACAAACA 3′	rev
BSS9	5′ GTTATATGTATGTATGTATGGGTGAT 3′	for
BSS10	5′ ACAAAAACACAAACAAACAAAT 3′	rev
BSS13	5′ TGAATTGGGATTGTTAGTTTTG 3′	for
BSS14	5′ CAATAACCRACACATAAATAACAAA 3′	rev
BSS15	5′ GGTTTGTTGTTTGTTTTTATTTTGT 3′	for
BSS16	5′ ACCRATCACCCATACATACATA 3′	rev
BSS17	5′ ATGATGAGTTTTAGGTAGGTTGA 3′	for
BSS18	5′ TTATCATAATAACATCRAACAACC 3′	rev
BSS23	5′ TGGAAGTTGTTGTTGTTGTGT 3′	for
BSS24	5′ AAACACRCACCTAAAACAAAAA 3′	rev

alone is not sufficient for hypermethylation and silencing of *R-r:std* (Walker 1998). Similar to *P1-rr*, DNA methylation of a regulatory sequence associated with a fragmented transposable element might cause *S1* and *S2* repression. In brief, transposable elements possibly make *P1-rr* and *R-r:std* susceptible to gene silencing and paramutation, and epigenetic modifications of the transposons such as methylation might spread into regulatory sequences of flanking genes resulting in transcriptional inactivation. However, a *doppia* fragment that does not affect paramutation was also found 129 bp upstream of the translational start site of the paramutable *Pl1-Rh* and the paramutagenic *Pl1′* alleles (Cone et al. 1993; Hollick 2010). Cytosine methylation in this *doppia* element did not vary between both epialleles (Erhard et al. 2009; Hale et al. 2007).

How many genes participate in paramutation in maize?

The majority of maize genes that have been shown to be epigenetically regulated are involved in the anthocyanin pathway. The readily visible phenotype of genes conferring anthocyanin pigmentation to plant tissue allows detection of even small expression changes. It is likely that many genes with no immediate visible phenotype undergo epigenetic silencing as well. Recent results obtained for the *lpa1* gene (Pilu et al. 2009) confirm that epigenetically regulated genes are not confined to the anthocyanin biosynthesis pathway. *lpa1* encodes a transporter in the essential phytic acid pathway. Not surprisingly, extreme cases of gene silencing at *lpa1* are lethal to the organism. Repressed epialleles of essential genes will be more difficult to detect since they will readily be eliminated from the gene pool.

On the contrary, the active *B-I* allele is only viable through constant human selection because *B-I* spontaneously and in a heterozygote with *B′* converts to the low expression state of *B′*. It is conceivable that the single phenomenon known as paramutation is the result of several, possibly independent mechanisms as shown for instance by the different effects of mutant genes (Pilu et al. 2009; Sidorenko et al. 2009). However, if paramutation is linked to transposon silencing as we have proposed here for *P1-pr* then the amount of epialleles and paramutable alleles could correlate with the quantity of transposable elements in the genome. With the maize genome consisting of a large percentage of transposons (Messing et al. 2004), we expect to discover more epialleles in the future that are possibly also of agronomic importance. Ultimately, our understanding of epigenetic gene regulation of maize will undoubtedly be beneficial for transgenic applications ensuring that corn continues to be an important food and energy source worldwide.

References

Alleman M, Sidorenko L, McGinnis K, Seshadri V, Dorweiler JE, White J, Sikkink K, Chandler VL (2006) An RNA-dependent RNA polymerase is required for paramutation in maize. Nature 442:295–298

Arteaga-Vazquez MA, Chandler VL (2010) Paramutation in maize: RNA mediated trans-generational gene silencing. Curr Opin Genet Dev 20:156–163

Arteaga-Vazquez M, Sidorenko L, Rabanal FA, Shrivistava R, Nobuta K, Green PJ, Meyers BC, Chandler VL (2010) RNA-mediated trans-communication can establish paramutation at the b1 locus in maize. Proc Nat Acad Sci USA 107:12986–12991

Athma P, Peterson T (1991) Ac induces homologous recombination at the maize P locus. Genetics 128:163–173

Bateson W, Pellew C (1915) On the genetics of 'rogues' among culinary peas (*Pisum sativum*). J Genet 5:15–36

Brink RA (1956) A genetic change associated with the R locus in maize which is directed and potentially reversible. Genetics 41:872–890

Brink RA (1958) Paramutation at the R locus in maize. Cold Spring Harbor Symp Quant Biol 23:379–391

Brink RA (1973) Paramutation. Annu Rev Genet 7:129–152

Chandler VL (2010) Paramutation's properties and puzzles. Science (New York, NY) 330:628–629

Chandler VL, Stam M (2004) Chromatin conversations: mechanisms and implications of paramutation. Nat Rev Genet 5:532–544

Chandler VL, Eggleston WB, Dorweiler JE (2000) Paramutation in maize. Plant Mol Biol 43:121–145

Chopra S, Cocciolone SM, Bushman S, Sangar V, McMullen MD, Peterson T (2003) The maize unstable factor for orange1 is a dominant epigenetic modifier of a tissue specifically silent allele of pericarp color1. Genetics 163:1135–1146

Coe EH (1966) The properties, origin, and mechanism of conversion-type inheritance at the B locus in maize. Genetics 53:1035–1063

Colot V, Maloisel L, Rossignol JL (1996) Interchromosomal transfer of epigenetic states in Ascobolus: transfer of DNA methylation is mechanistically related to homologous recombination. Cell 86:855–864

Cone KC, Cocciolone SM, Moehlenkamp CA, Weber T, Drummond BJ, Tagliani LA, Bowen BA, Perrot GH (1993) Role of the regulatory gene pl in the photocontrol of maize anthocyanin pigmentation. Plant Cell 5:1807–1816

Cuzin F, Grandjean V, Rassoulzadegan M (2008) Inherited variation at the epigenetic level: paramutation from the plant to the mouse. Curr Opin Genet Dev 18:193–196

Das OP, Messing J (1994) Variegated phenotype and developmental methylation changes of a maize allele originating from epimutation. Genetics 136:1121–1141

Dooner HK, He L (2008) Maize genome structure variation: interplay between retrotransposon polymorphisms and genic recombination. Plant Cell 20:249–258

Dorweiler JE, Carey CC, Kubo KM, Hollick JB, Kermicle JL, Chandler VL (2000) mediator of paramutation1 is required for establishment and maintenance of paramutation at multiple maize loci. Plant Cell 12:2101–2118

Du C, Hoffman A, He L, Caronna J, Dooner HK (2011) The complete Ac/Ds transposon family of maize. BMC genomics 12:588

Ehlert B, Schottler MA, Tischendorf G, Ludwig-Muller J, Bock R (2008) The paramutated SULFUREA locus of tomato is involved in auxin biosynthesis. J Exp Bot 59:3635–3647

Erhard KF Jr, Hollick JB (2011) Paramutation: a process for acquiring trans-generational regulatory states. Curr Opin Plant Biol 14:210–216

Erhard KF Jr, Stonaker JL, Parkinson SE, Lim JP, Hale CJ, Hollick JB (2009) RNA polymerase IV functions in paramutation in *Zea mays*. Science (New York, NY) 323:1201–1205

Goettel W, Messing J (2009) Change of gene structure and function by non-homologous end-joining, homologous recombination, and transposition of DNA. PLoS Genet 5:e1000516

Goettel W, Messing J (2010) Divergence of gene regulation through chromosomal rearrangements. BMC Genomics 11:678

Grandjean V, Gounon P, Wagner N, Martin L, Wagner KD, Bernex F, Cuzin F, Rassoulzadegan M (2009) The miR-124-Sox9 paramutation: RNA-mediated epigenetic control of embryonic and adult growth. Development (Cambridge, England) 136:3647–3655

Grotewold E, Athma P, Peterson T (1991) A possible hot spot for Ac insertion in the maize P gene. Mol Gen Genet 230:329–331

Haag JR, Pikaard CS (2011) Multisubunit RNA polymerases IV and V: purveyors of non-coding RNA for plant gene silencing. Nat Rev 12:483–492

Hale CJ, Stonaker JL, Gross SM, Hollick JB (2007) A novel Snf2 protein maintains trans-generational regulatory states established by paramutation in maize. PLoS Biol 5:2156–2165

Haring M, Bader R, Louwers M, Schwabe A, van Driel R, Stam M (2010) The role of DNA methylation, nucleosome occupancy and histone modifications in paramutation. Plant J 63(3): 366–378

Hollick JB (2010) Paramutation and development. Annu Rev Cell Dev Biol 26:557–579

Hollick JB, Patterson GI, Coe EH, Cone KC, Chandler VL (1995) Allelic interactions heritably alter the activity of a metastable maize pl allele. Genetics 141:709–719

Kermicle JL, Eggleston WB, Alleman M (1995) Organization of paramutagenicity in R-stippled maize. Genetics 141:361–372

Krebbers E, Hehl R, Piotrowiak R, Lonnig WE, Sommer H, Saedler H (1987) Molecular analysis of paramutant plants of *Antirrhinum majus* and the involvement of transposable elements. Mol Gen Genet 209:499–507

Law JA, Jacobsen SE (2010) Establishing, maintaining and modifying DNA methylation patterns in plants and animals. Nat Rev Genet 11:204–220

Lisch D, Carey CC, Dorweiler JE, Chandler VL (2002) A mutation that prevents paramutation in maize also reverses Mutator transposon methylation and silencing. Proc Nat Acad Sci USA 99:6130–6135

Louwers M, Bader R, Haring M, van Driel R, de Laat W, Stam M (2009) Tissue- and expression level-specific chromatin looping at maize b1 epialleles. Plant Cell 21:832–842

Lund G, Das OP, Messing J (1995) Tissue-specific DNase-I-sensitive sites of the maize p-gene and their changes upon epimutation. Plant J 7(5):797–807

Maloisel L, Rossignol JL (1998) Suppression of crossing-over by DNA methylation in Ascobolus. Genes Dev 12:1381–1389

Martienssen R (1996) Epigenetic phenomena: paramutation and gene silencing in plants. Curr Biol 6:810–813

McGinnis KM, Springer C, Lin Y, Carey CC, Chandler V (2006) Transcriptionally silenced transgenes in maize are activated by three mutations defective in paramutation. Genetics 173: 1637–1647

Messing J, Bharti AK, Karlowski WM, Grundlach H, Kim HR, Yu Y, Wei F, Fuks G, Soderlund CA, Mayer KFX, Wing RA (2004) Sequence composition and genome organization of maize. Proc Nat Acad Sci USA 101:14349–14354

Meyer P, Heidmann I, Niedenhof I (1993) Differences in DNA-methylation are associated with a paramutation phenomenon in transgenic petunia. Plant J 4:89–100

Mittelsten Scheid O, Afsar K, Paszkowski J (2003) Formation of stable epialleles and their paramutation-like interaction in tetraploid *Arabidopsis thaliana*. Nat Genet 34:450–454

Nobuta K, Lu C, Shrivastava R, Pillay M, De Paoli E, Accerbi M, Arteaga-Vazquez M, Sidorenko L, Jeong DH, Yen Y, Green PJ, Chandler VL, Meyers BC (2008) Distinct size distribution of endogeneous siRNAs in maize: evidence from deep sequencing in the mop1-1 mutant. Proc Nat Acad Sci USA 105:14958–14963

Panavas T, Weir J, Walker EL (1999) The structure and paramutagenicity of the R-marbled haplotype of *Zea mays*. Genetics 153:979–991

Pilu R, Panzeri D, Cassani E, Cerino Badone F, Landoni M, Nielsen E (2009) A paramutation phenomenon is involved in the genetics of maize low phytic acid1-241 (lpa1-241) trait. Heredity 102: 236–245

Rassoulzadegan M, Grandjean V, Gounon P, Vincent S, Gillot I, Cuzin F (2006) RNA-mediated non-mendelian inheritance of an epigenetic change in the mouse. Nature 441:469–474

Rassoulzadegan M, Grandjean V, Gounon P, Cuzin F (2007) Inheritance of an epigenetic change in the mouse: a new role for RNA. Biochem Soc Trans 35:623–625

Robbins ML, Wang P, Sekhon RS, Chopra S (2009) Gene structure induced epigenetic modifications of pericarp color1 alleles of maize result in tissue-specific mosaicism. PLoS ONE 4:e8231

Sekhon RS, Chopra S (2009) Progressive loss of DNA methylation releases epigenetic gene silencing from a tandemly repeated maize Myb gene. Genetics 181:81–91

Sekhon RS, Peterson T, Chopra S (2007) Epigenetic modifications of distinct sequences of the p1 regulatory gene specify tissue-specific expression patterns in maize. Genetics 175:1059–1070

Sidorenko L, Chandler V (2008) RNA-dependent RNA polymerase is required for enhancer-mediated transcriptional silencing associated with paramutation at the maize p1 gene. Genetics 180: 1983–1993

Sidorenko LV, Peterson T (2001) Transgene-induced silencing identifies sequences involved in the establishment of paramutation of the maize p1 gene. Plant Cell 13:319–335

Sidorenko LV, Li X, Cocciolone SM, Chopra S, Tagliani L, Bowen B, Daniels M, Peterson T (2000) Complex structure of a maize Myb gene promoter: functional analysis in transgenic plants. Plant J 22:471–482

Sidorenko L, Dorweiler JE, Cigan AM, Arteaga-Vazquez M, Vyas M, Kermicle J, Jurcin D, Brzeski J, Cai Y, Chandler VL (2009) A dominant mutation in mediator of paramutation2, one of three second-largest subunits of a plant-specific RNA polymerase, disrupts multiple siRNA silencing processes. PLoS Genet 5:e1000725

Stam M, Belele C, Dorweiler JE, Chandler VL (2002) Differential chromatin structure within a tandem array 100 kb upstream of the maize b1 locus is associated with paramutation. Genes Dev 16:1906–1918

Stokes TL, Richards EJ (2002) Induced instability of two Arabidopsis constitutive pathogen-response alleles. Proc Natl Acad Sci USA 99:7792–7796

Stonaker JL, Lim JP, Erhard KF Jr, Hollick JB (2009) Diversity of Pol IV function is defined by mutations at the maize rmr7 locus. PLoS Genet 5:e1000706

Wagner KD, Wagner N, Ghanbarian H, Grandjean V, Gounon P, Cuzin F, Rassoulzadegan M (2008) RNA induction and inheritance of epigenetic cardiac hypertrophy in the mouse. Dev Cell 14:962–969

Walbot V (2001) Imprinting of R-r, paramutation of B-I and Pl, and epigenetic silencing of MuDR/Mu transposons in *Zea mays* L. are coordinately affected by inbred background. Genet Res 77:219–226

Walker EL (1998) Paramutation of the r1 locus of maize is associated with increased cytosine methylation. Genetics 148:1973–1981

Worch S, Hansmann I, Schlote D (2008) Paramutation-like effects at the mouse scapinin (Phactr3) locus. J Mol Biol 377:605–608

Yam KL, Papadakis SE (2004) A simple digital imaging method for measuring and analyzing color of food surfaces. J Food Eng 61:137–142